CHIN. PHYS. LETT. Vol. 35, No. 2 (2018) 026101

Effects of Grain Boundary Characteristics on Its Capability to Trap Point Defects in Tungsten *

Wen-Hao He(何文豪)[1,2], Xing Gao(高星)[1**], Ning Gao(高宁)[1], Ji Wang(王雱)[3], Dong Wang(王栋)[4], Ming-Huan Cui(崔明焕)[1], Li-Long Pang(庞立龙)[1], Zhi-Guang Wang(王志光)[1**]

[1]*Institute of Modern Physics, Chinese Academy of Sciences, Lanzhou 730000*
[2]*University of Chinese Academy of Sciences, Beijing 100049*
[3]*Ningbo Institute of Industrial Technology, Chinese Academy of Sciences, Ningbo 315201*
[4]*State Key Laboratory of New Ceramics and Fine Processing, School of Materials Science and Engineering, Tsinghua University, Beijing 100084*

(Received 2 November 2017)

As recombination centers of vacancies (Vs) and self-interstitial atoms (SIAs), firstly grain boundaries (GBs) should have strong capability of trapping point defects. In this study, abilities to trap Vs and SIAs of eight symmetric tilt GBs in tungsten are investigated through first-principles calculations. On the one hand, vacancy formation energy $E_{\rm V}^{\rm f}$ rapidly increases then slowly decreases as the hard-sphere radius r_0 of the vacancy increases. The value of $E_{\rm V}^{\rm f}$ is the largest when r_0 is about 1.38 Å, which is half the distance between the nearest atoms in equilibrium single crystal tungsten. That is, any denser or looser atomic configuration around GBs than that in bulk is helpful to form a vacancy. On the other hand, SIA formation energy $E_{\rm SIA}^{\rm f}$ at GBs decreases monotonically with increasing the hard-sphere radius of the interstitial sites, which indicates that GBs with larger interstitial sites have stronger ability to trap SIAs. Based on the data obtained for GBs investigated in this study, it is found that the ability to trap Vs increases as the GB energy increases, and the capability of trapping SIAs linearly increases as the excess volume of GB increases. Due to its lowest GB energy and smallest excess volume among all GBs studied, twin GB $\sum$3(110)[111] has the weakest capability to trap both Vs and SIAs.

PACS: 61.72.jd, 61.72.jj, 61.72.Mm DOI: 10.1088/0256-307X/35/2/026101

Materials serving in nuclear energy systems are usually exposed to high irradiation doses of particles. Projectile particles lead to creations of a large numbers of vacancies (Vs) and self-interstitial atoms (SIAs) in materials. The SIAs may gather to form dislocation loops and stacking-fault tetrahedrons, and the Vs usually gather to form voids. These defects contribute to materials swelling, hardening, amorphization and embrittlement, and may accelerate material failure under irradiation.[1–9] To enhance radiation resistance of materials and to extend operating time of nuclear energy systems, it is essential to develop materials to suppress accumulations of point defects of the same type and to enhance annihilations of Vs and SIAs. Extensive experimental results demonstrated that nano-crystalline materials generally show better radiation resistance than common poly-crystalline materials because of a higher fraction of grain boundaries (GBs) in the nano-crystalline materials.[10–14] To understand the role played by a GB in annihilations of point defects, a large number of computer simulations have been carried out. First-principles calculations indicated that Vs and SIAs could easily segregate to tungsten GB regions.[15] Molecular statics simulations at 0 K showed that SIAs and Vs are thermodynamically favorable to aggregate at GBs.[16–19] Molecular dynamics simulations demonstrated that grain boundaries act as sinks of highly efficient point defects that could not saturate even under extreme radiation conditions.[20–22]

Although GBs are commonly identified to be point-defect sinks and recombination centers, threshold stresses in Nabarro–Herring creep provide the earliest indication that point-defect sink strengths might depend on GB structures.[23] More direct confirmation of such dependence was obtained by measuring the widths of void-denuded zones near different GBs in irradiated metals or metals quenched from high temperatures.[24–26] Among all those identified GBs, the vacancy sink efficiency of twin boundary $\sum$3(110)[111] is found to be significantly lower than that of other GBs.[24–26] Moreover, nano-crystalline copper containing a high fraction of twin boundary $\sum$3(110)[111] shows no enhancement in radiation resistance.[27] Usually, GBs with high abilities to trap point defects and to annihilate Frenkel pair will be good sinks for Vs and SIAs. In this Letter, we mainly focus on effects of atomic configurations around GBs on their ability to trap Vs and SIAs.

Tungsten is one of the promising candidates for plasma facing materials (PFMs), such as the first wall materials and divertor of magnetic confinement fusion reactor due to its high melting temperature, high thermal conductivity and low sputtering erosion. In our following study, abilities to trap Vs and SIAs of eight symmetric tilt GBs in tungsten are investigated through first-principles calculations. The eight symmetric tilt GBs are constructed by the coincidence site lattice (CSL) model.[28] Formation energies of Vs and SIAs at the eight symmetrical tilt GBs are computed. Effects of GB characteristics on their abilities to trap Vs and SIAs at these eight symmetric tilt GBs in tung-

*Supported by the National Natural Science Foundation of China under Grant Nos 91426301, 11605256 and 11405231.
**Corresponding author. Email: xinggao@impcas.ac.cn; zhgwang@impcas.ac.cn
© 2018 Chinese Physical Society and IOP Publishing Ltd

sten are discussed.

First-principles total energy calculations[29] are carried out with the Vienna ab initio simulation package (VASP)[30–32] based on the density functional theory (DFT).[33,34] The projected augmented wave (PAW)[35] pseudopotentials are employed in the calculations within the generalized gradient approximation (GGA) with Perdew and Wang[36] functional for the exchange and correlation energies. A cutoff energy of 400 eV is used for the plane-wave expansion. The internal structural relaxations are stopped when the residual force on each atom is less than 0.01 eV/Å. Both atomic positions and volumes of supercells are allowed to relax in all the calculations.

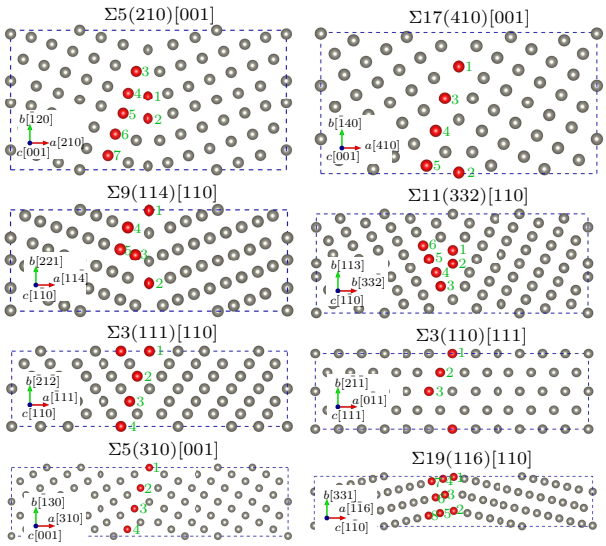

Fig. 1. Schematic illustration of vacancies around all GBs studied here. Grey balls refer to tungsten atoms, and red balls marked with numbers refer to vacancies.

By least-square-fitting total energies to the 4th Murnaghan equation of state, our calculated equilibrium lattice constant of the body centered cubic tungsten is 3.19 Å, which is slightly overestimated as compared with the experimental data of 3.165 Å.[37] A $4 \times 4 \times 4$ supercell (128 atoms) with the calculated lattice parameter is employed to calculate the formation energies of V and SIA in the bulk. Constructions of the eight symmetric tilt GBs in tungsten as well as choices of k-meshes are the same as those in our previous study.[38] According to the investigation of Chai *et al.*, the difference of the vacancy formation energy in bulk tungsten and at sites larger than 3.19 Å away from GB $\sum 5(310)[001]$ plane is within 0.23 eV.[15] Our calculations also show that the vacancy formation energies at sites about 3.19 Å away from GBs are close to that in the bulk. This can be attributed to the fact that the environment around these vacancies becomes closer to that in the bulk as the distance away from the GB plane increases. Therefore, in this study, only those sites within about 3.19 Å from GB plane are considered to explore their vacancy formation energies. Figure 1 shows the diagram of Vs around all GBs studied here. Different numbers refer to different Vs. The distance from the V to the GB plane increases as the number increases for each GB. The vacancy formation energy $E_{\mathrm{V}}^{\mathrm{f}}$ at each site around GBs (in bulk) can be calculated by

$$E_{\mathrm{V}}^{\mathrm{f}} = E_{\mathrm{GB(bulk),V}} - E_{\mathrm{GB(bulk)}} + e_{\mathrm{W}}, \qquad (1)$$

where $E_{\mathrm{GB(bulk),V}}$ is the total energy of the supercell containing a vacancy around the GB (in the bulk), $E_{\mathrm{GB(bulk)}}$ is the total energy of the supercell containing the clean GB (bulk), and e_{W} is the energy of a tungsten atom in bulk environment.

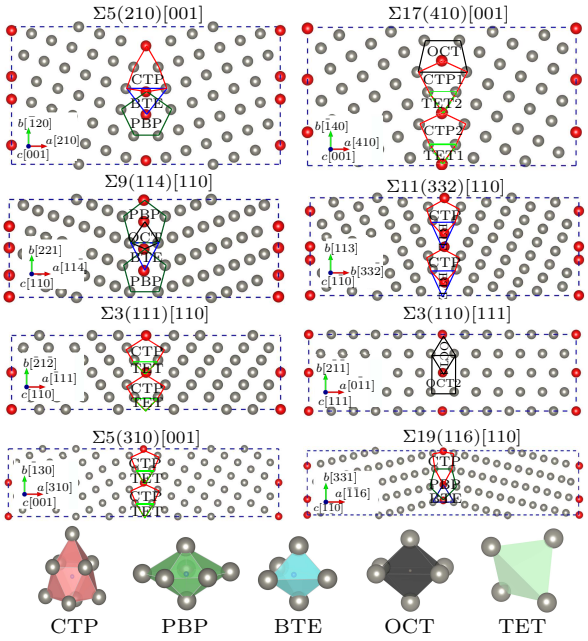

Fig. 2. Schematic illustration of polyhedral interstitial sites at GB planes. Red, dark green, blue, black and bright green polyhedra refer to CTP, PBP, BTE, OCT and TET respectively. Grey balls refer to tungsten atoms, and red balls refer to tungsten atoms at GB planes.

To calculate SIA formation energy, interstitial sites must be identified firstly. In general, larger interstitial sites are located at the GB plane rather than regions near the GB plane, and atoms are easier to occupy larger interstitial sites. Thus we assume that SIA will take the sites at the GB plane. In fact, our calculations show that an SIA with ⟨111⟩ configuration initially added into a site near the GB plane spontaneously moves into the GB plane during relaxation. Moreover, Chai *et al.* also showed that the SIA could instantly segregate into GB $\sum 5(310)[001]$ via a barrier-free process and is located at the GB plane in tungsten when the distance between the SIA and the GB is shorter than 6.19 Å.[15] Therefore, only the interstitial sites at the GB planes are considered in our following study. As with our previous study,[38] GB structures are described with a series of convex deltahedra. This method has been employed to investigate GB related properties in materials, such as solutions and segregation of impurity elements at GBs.[39,40] As shown in Fig. 2, there are five types of polyhedral interstitial sites at the GB planes studied here, and they are tetrahedron (TET), octahedron (OCT), pentagonal bipyramid (PBP), cap trigonal prism (CTP) and

bitetrahedron (BTE). The SIA formation energy $E^{\rm f}_{\rm SIA}$ in each interstitial site at GBs (bulk) can be calculated by

$$E^{\rm f}_{\rm SIA} = E_{\rm GB(bulk),SIA} - E_{\rm GB(bulk)} - e_{\rm W}, \qquad (2)$$

where $E_{\rm GB(bulk),SIA}$ is the total energy of the supercell containing an SIA at GB (bulk).

To check the supercell size effect on the point defect formation energy, we take GB $\sum$11(332)[110] as an example to calculate $E^{\rm f}_{\rm V}$ at V1 and $E^{\rm f}_{\rm SIA}$ at CTP with different supercell sizes and the results are listed in Table 1. It can be seen that the differences of both $E^{\rm f}_{\rm V}$ and $E^{\rm f}_{\rm SIA}$ between different supercell sizes are relatively small. To ensure accuracies of these energies, the larger supercell is applied for GB $\sum$11(332)[110] in this study. For all other GBs, the supercell sizes along their shortest axis are all larger than 5.26 Å. Therefore, we believe that the supercell sizes used in this study are large enough to investigate the point defect formation energies at these GBs.

Table 1. Vacancy formation energies $E^{\rm f}_{\rm V}$, SIA formation energies $E^{\rm f}_{\rm SIA}$, numbers of atoms, k-meshes as well as the sizes for different supercells for GB $\sum$11(332)[110].

Systems	Number of atoms	k-mesh	L_a (Å)	L_b (Å)	L_c (Å)	Sites	$E^{\rm f}_{\rm V}$	Sites	$E^{\rm f}_{\rm SIA}$
$\sum$11(332)[110]	84	1×5×3	29.12	5.26	9.03	V1	2.47	CTP	2.77
$\sum$11(332)[110]	168	1×3×3	29.10	10.53	9.03	V1	2.54	CTP	2.71

Table 2. Vacancy formation energies $E^{\rm f}_{\rm V}$ in bulk and the eight symmetric tilt GBs studied here. These vacancy sites are labelled as shown in Fig. 1.

System	Vacancy formation energy $E^{\rm f}_{\rm V}$ (eV)							
	V1	V2	V3	V4	V5	V6	V7	V8
Bulk	3.19 (3.11[a], 3.1–4.0[b])							
$\sum$3(110)[111]	3.40	2.74	3.18					
$\sum$3(111)[110]	3.34	1.25	2.34	3.55				
$\sum$5(310)[001]	3.29 (3.18[c])	1.75 (1.58[c])	2.99 (2.90[c])	2.77 (2.64[c])				
$\sum$5(210)[001]	1.49	2.95	0.87	0.69	1.05	1.05	1.86	
$\sum$9(114)[110]	1.88	2.58	2.25	2.15	2.99			
$\sum$11(332)[110]	2.54	1.81	1.37	2.21	1.81	2.43		
$\sum$17(410)[001]	3.14	2.48	2.13	2.31	2.40			
$\sum$19(116)[110]	2.98	2.69	−0.15	2.83	−0.15	−1.09	−0.15	3.26

[a]Ref. [41], [b]Ref. [42], and [c]Ref. [15].

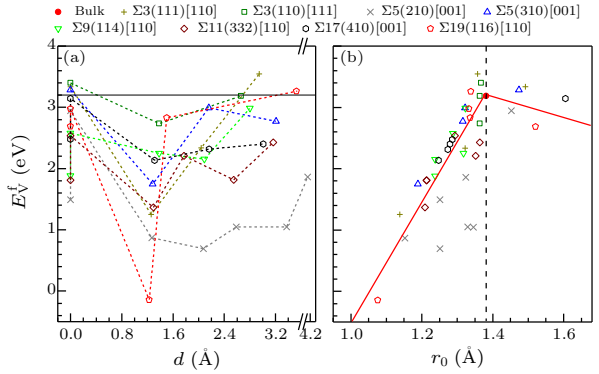

Fig. 3. (a) Vacancy formation energy $E^{\rm f}_{\rm V}$ versus distance d from the center of the vacancy to the GB plane. The black horizontal solid line refers to the vacancy formation energy in bulk, and (b) $E^{\rm f}_{\rm V}$ versus hard-sphere radius r_0 of the vacancy. The red solid line is drawn to guide the eyes. The black vertical dashed line refers to the hard-sphere radius of 1.38 Å.

The vacancy formation energies $E^{\rm f}_{\rm V}$ around the eight GBs and in bulk are listed in Table 2. The value of $E^{\rm f}_{\rm V}$ in bulk is 3.19 eV, in line with the value of 3.11 eV reported in Ref. [41] and the experimental data of 3.1–3.4 eV reported by Maier *et al.*[42] Our calculated $E^{\rm f}_{\rm V}$ around GB $\sum$5(310)[001] also agree with the data reported.[15] It is noted that the initial vacancies at sites V5 and V7 move spontaneously to V3 for GB $\sum$19(116)[110] during atomic configuration relaxation. As for the vacancy site V6 at GB $\sum$19(116)[110], in addition to the atoms around the vacancy, atoms in several layers far from the vacancy site obviously deviate from their original sites during relaxation, and the final atomic configuration changes quite a bit. Therefore, in the following the V6 at GB $\sum$19(116)[110] will be excluded.

Figure 3(a) shows the relationship between $E^{\rm f}_{\rm V}$ and distance d from the center of the vacancy to the GB plane. It can be seen that $E^{\rm f}_{\rm V}$ decreases first then increases for each GB as d increases. The value of $E^{\rm f}_{\rm V}$ will be gradually closer to that in bulk as the distance d increases further, which can be attributed to the fact that the environment around the vacancy becomes closer to that in bulk as d increases. The black horizontal solid line refers to $E^{\rm f}_{\rm V}$ in bulk. Clearly, most $E^{\rm f}_{\rm V}$'s around GBs are lower than that in bulk. This means that the Vs can be easily trapped by GBs. To understand the large variation of the vacancy formation energy in different GB systems, $E^{\rm f}_{\rm V}$ versus hard-sphere radius r_0 of the vacancy is shown in Fig. 3(b). Here r_0 is defined as the largest hard-sphere radius which can be inserted into the vacancy. The hard-sphere radius of tungsten atom is defined as half the distance between the nearest neighbors in bcc tungsten, which is 1.38 Å in equilibrium bcc tungsten. As shown in Fig. 3(b), $E^{\rm f}_{\rm V}$ increases rapidly as r_0 increases and reaches its largest value as r_0 reaches 1.38 Å. Then $E^{\rm f}_{\rm V}$ decreases slowly as r_0 keeps increasing. This result is reasonably sound since the binding energy in bcc tungsten is the largest when the first nearest neighbor distance is 2.76 Å. Any shorter or longer distance

between them will induce the decrease of the binding energy thus make the formation of a vacancy easier. Here r_0 can refer to the atomic density around GB. The smaller the r_0 is, the larger the atomic density is. According to the relation between E_V^f and r_0, it is easily found that any denser or looser atomic configuration around GB than that in bulk is helpful to form a vacancy, that is, the ability of the GB to trap Vs is stronger.

To calculate SIA formation energies, atomic configurations of GBs with SIAs are relaxed firstly. For GB $\sum$17(410)[001], it is found that the SIA initially added into OCT site would spontaneously move into CTP site during atomic relaxations, which indicates that migration of SIA from the OCT to the CTP is remarkably easy. Similar phenomena are observed in GB $\sum$3(111)[110], GB $\sum$9(114)[110] and GB $\sum$19(116)[110]. For GB $\sum$3(111)[110], a TET SIA moves into a CTP. For GB $\sum$9(114)[110], the SIA in an OCT, and a BTE moves into a PBP. As for GB $\sum$19(116)[110], the SIA in a BTE moves into a CTP.

Like all nonmagnetic bcc transition metals, the $\langle 111\rangle$-type configuration of SIAs has the lowest formation energies in tungsten.[43] In this study, E_{SIA}^f of the $\langle 111\rangle$ dumbbell is lower than that of the $\langle 111\rangle$ crowd ion by 2 meV and the lowest E_{SIA}^f is 9.90 eV, which agrees with the value of 9.94 eV reported in the previous study.[41] The relationship between E_{SIA}^f around GBs and hard-sphere radius r_0 of the interstitial site is shown in Fig. 4. As with the hard-sphere radius defined for vacancy, r_0 of an interstitial site is defined as the largest hard-sphere radius that can be added into the interstitial site. The black horizontal solid line refers to the $\langle 111\rangle$ dumbbell formation energy in bulk. Clearly, most E_{SIA}^f's at GBs are lower than that in the bulk. This can be attributed to the relatively larger interstitial site at GBs. In addition, E_{SIA}^f at GBs decreases as the hard-sphere radius r_0 of the interstitial increases. According to the relationship between E_{SIA}^f and r_0, it is easily found that the larger interstitial site at GBs is more helpful to accommodate SIA, that is, GBs containing larger interstitial sites have stronger ability to trap SIAs.

In general, the segregation energy $E_{V(SIA)}^S$ of V(SIA) is used to indicate GB capability to trap intrinsic point defects. The Vs and SIAs will prefer to segregate to sites with the lowest formation energy. Accordingly, $E_{V(SIA)}^S$ at a GB can be defined as

$$E_{V(SIA)}^S = E_{GB,V(SIA)}^f - E_{Bulk,V(SIA)}^f, \quad (3)$$

where $E_{GB,V(SIA)}^f$ and $E_{Bulk,V(SIA)}^f$ are the lowest formation energy of V(SIA) at the GB and in bulk, respectively. The larger the segregation energy is, the less easily the point defect segregates to the GB. The values of $E_{V(SIA)}^S$ for the eight symmetric tilt GBs are listed in Table 3. Clearly, the segregation energies of V and SIA differ for different GBs. Among all eight GBs studied here, both the segregation energies of V and SIA for the twin GB $\sum$3(110)[111] are the largest, which means that the twin GB $\sum$3(110)[111] is less favorable to segregation of Vs and SIAs.

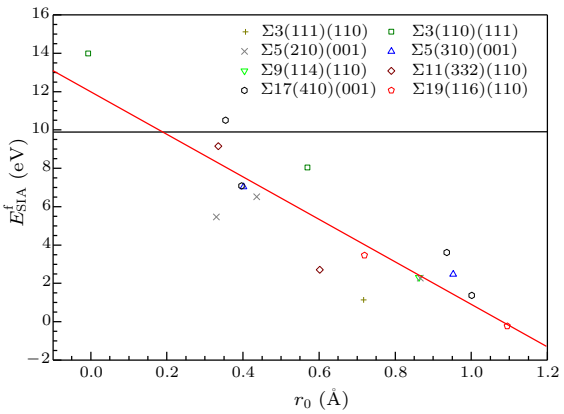

Fig. 4. SIA formation energies E_{SIA}^f versus hard-sphere radius r_0 of interstitial sites. The red solid line is drawn to guide the eyes. The black horizontal solid line refers to the formation energy of $\langle 111\rangle$ dumbbell in bulk.

Table 3. Segregation energies $E_{V(SIA)}^S$ of V(SIA) at the eight symmetric tilt GBs studied here.

Systems	Segregation energy (eV)		Systems	Segregation energy (eV)	
	E_V^S	E_{SIA}^S		E_V^S	E_{SIA}^S
$\sum$3(110)[111]	−0.45	−1.87	$\sum$9(114)[110]	−1.31	−7.60
$\sum$3(111)[110]	−1.93	−8.78	$\sum$11(332)[110]	−1.82	−7.21
$\sum$5(310)[001]	−1.44	−7.44	$\sum$17(410)[001]	−1.05	−8.53
$\sum$5(210)[001]	−2.49	−7.64	$\sum$19(116)[110]	−3.33	−10.14

According to our results shown above, the denser or looser the atomic configurations around GB than that in bulk are, the easier it is to form a vacancy. On the other hand, it is obvious that the more the lattice distortion of GB is, the higher the grain boundary energy γ is. Thus it is reasonable to assume that the higher the grain boundary energy is, the lower the vacancy formation energy is. Figure 5(a) shows the relationship between E_V^S and γ. These grain boundary energies have been reported in our previous study.[38] It can be seen that E_V^S decreases as γ increases. Furthermore, larger interstitial site at GBs is more helpful to accommodate SIA. That is, GBs with larger excess volume V_{GB}/S might have stronger capability of trapping SIA. The value of V_{GB}/S of a GB is defined as[44]

$$V_{GB}/S = \left(V - \frac{V_0}{n_0} \times n\right)/(2 \times S), \quad (4)$$

where V_0 and n_0 are volume and number of atoms in perfect bulk, V, n and S are volume, number of atoms and cross sectional area in supercell containing the GB, respectively. Figure 5(b) shows the relationship between E_{SIA}^S and V_{GB}/S. It is obvious that E_{SIA}^S monotonically decreases as V_{GB}/S increases. Among

all our studied GBs, GB $\sum$19(116)[110] is the best trapping center for both Vs and SIAs. Thus this GB may be a good recombination center since stronger ability to trap both Vs and SIAs will provide higher possibility for recombination of Vs and SIAs at or near the GB.

Compared with experimental investigations, which have shown that vacancy sink efficiency varies for different GBs and the twin GB $\sum$3(110)[111] has lower vacancy sink efficiency,[24–26] our calculations also show that the ability to trap Vs and SIAs varies for different GBs. Among all GBs investigated in this study, the ability of the twin GB $\sum$3(110)[111] to trap both Vs and SIAs is the weakest due to its lowest GB energy and smallest excess volume.

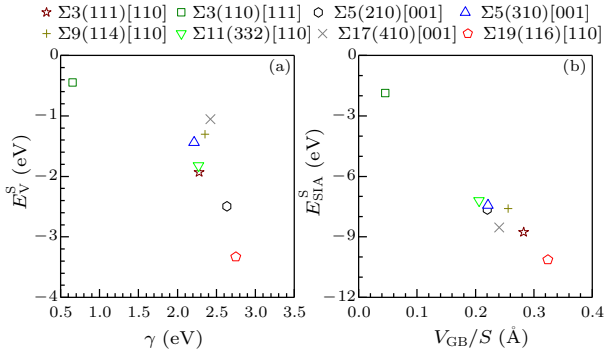

Fig. 5. Dependence of segregation energy E_V^S of V on GB energy γ (a) and E_{SIA}^S of SIA on excess volume V_{GB}/S of GB (b).

In summary, formation energies and segregation energies of V and SIA at eight symmetric tilt GBs in tungsten have been investigated through the first-principles calculations. Firstly, effect of GB morphology on the formation energy of V and SIA is analyzed. The vacancy formation energy rapidly increases and then slowly decreases as the hard-sphere radius r_0 of the vacancy increases. The value of E_V^f is the largest when r_0 is equal to about 1.38 Å, which is half the distance between the nearest tungsten atoms in body center cubic tungsten. Regarding to the formations of SIAs at GBs, the formation energies decrease monotonously as the hard-sphere radii of the interstitial sites increase. The larger interstitial site at GB is more helpful to accommodate SIA. Then, effect of GB characteristics, especially GB energy and excess volume, on the GB ability to trap Vs and SIAs is discussed. The ability to trap Vs increases as the GB energy increases, and the capability to trap SIAs linearly increases as the excess volume of the GB increases. Among all the GBs studied here, the twin GB $\sum$3(110)[111] has the weakest capability to trap Vs and SIAs due to its lowest GB energy and smallest excess volume.

References

[1] Trinkaus H and Wolfer W G 1984 *J. Nucl. Mater.* **122** 552
[2] Stubbins J F 1986 *J. Nucl. Mater.* **141** 748
[3] Singh B N, A Foreman J E and Trinkaus H 1997 *J. Nucl. Mater.* **249** 103
[4] Sickafus K E, Grimes R W, Valdez J A et al 2007 *Nat. Mater.* **6** 217
[5] Odette G R and Lucas G E 1998 *Radiat. Eff. Defects Solids* **144** 189
[6] Zinkle S J and Ghoniem N M 2000 *Fusion Eng. Des.* **51** 55
[7] Victoria M, Baluc N, Bailat C et al 2000 *J. Nucl. Mater.* **276** 114
[8] Diaz de la Rubia T, Zbib H M, Khraishi T A et al 2000 *Nature* **406** 871
[9] Odette G R and Lucas G E 2001 *JOM* **53** 18
[10] Kurishita H, Kobayashi S, Nakai K et al 2008 *J. Nucl. Mater.* **377** 34
[11] Fukuda M, Hasegawa A, Tanno T et al 2013 *J. Nucl. Mater.* **442** S273
[12] Kurishita H, Matsuso S, Arakawa H et al 2009 *Adv. Mater. Res.* **59** 18
[13] Kurishita H, Kobayashi S, Nakai K et al 2007 *Phys. Scr.* **T128** 76
[14] Kurishita H, Amano Y, Kobayashi S et al 2007 *J. Nucl. Mater.* **367** 1453
[15] Chai J, Li Y H, Niu L L et al 2017 *Nucl. Instrum. Methods Phys. Res. Sect.* B **393** 144
[16] Tschopp M A, Solanki K N, Gao F et al 2012 *Phys. Rev.* B **85** 064108
[17] Li X, Liu W, Xu Y et al 2013 *Nucl. Fusion* **53** 123014
[18] Li X, Liu W, Xu Y et al 2014 *J. Nucl. Mater.* **444** 229
[19] Bai X M, Voter A F, Hoagland R G et al 2010 *Science* **327** 1631
[20] Chen D, Wang J, Chen T et al 2013 *Sci. Rep.* **3** 1450
[21] Li X, Liu W, Xu Y et al 2016 *Acta Mater.* **109** 115
[22] Li X, Duan G, Xu Y et al 2017 *Nucl. Fusion* **57** 116055
[23] Ashby M F 1969 *Scr. Metall.* **3** 837
[24] Siegel R W, Chang S M and Balluffi R W 1980 *Acta Metall.* **28** 249
[25] Han W Z, Demkowiczand M J, Fu E G et al 2012 *Acta Mater.* **60** 6341
[26] Basu B K and Elbaum C 1965 *Acta Metall.* **13** 1117
[27] Demkowicz M J, Anderoglu O, Zhang X et al 2011 *J. Mater. Res.* **26** 1666
[28] King A H and Smith D A 1980 *Philos. Mag.* A **42** 495
[29] Perdew J P, Burke K and Ernzerhof M 1996 *Phys. Rev. Lett.* **77** 3865
[30] Kresse G and Hafner J 1993 *Phys. Rev.* B **47** 558
[31] Kresse G and Furthmuller J 1996 *Comput. Mater. Sci.* **6** 15
[32] Kresse G and Furthmuller J 1996 *Phys. Rev.* B **54** 11169
[33] Hohenberg P and Kohn W 1964 *Phys. Rev.* B **136** 864
[34] Gonze X, Ghosez Ph and Godby R W 1997 *Phys. Rev. Lett.* **78** 294
[35] Kresse G and Joubert D 1999 *Phys. Rev.* B **59** 1758
[36] Perdew J P and Wang Y 1992 *Phys. Rev.* B **45** 13244
[37] Kittel C 1996 *Introduction to Solid State Physics* (New York: John Wiley and Sons)
[38] He W H, Gao X, Wang D et al 2107 *Comput. Mater. Sci* (submitted)
[39] Baskes M I and Vitek V 1985 *Metall. Trans.* A **16** 1625
[40] Zhou X, Marchand D and McDowell D L 2016 *Phys. Rev. Lett.* **116** 075502
[41] Becquart C S and Domain C 2007 *Nucl. Instrum. Methods Phys. Res. Sect.* B **255** 23
[42] Maier K, Peo M, Saile B et al 1979 *Philos. Mag.* A **40** 701
[43] Nguyen-Manh D, Horsfield A P and Dudarev S L 2006 *Phys. Rev.* B **73** 020101(R)
[44] Kurtz R J and Heinisch H L 2004 *J. Nucl. Mater.* **329** 1199